THE JOURNAL OF PHYSICAL CHEMISTRY C

Article

Cite This: J. Phys. Chem. C 2018, 122, 26835−26844

pubs.acs.org/JPCC

Electronic and Vibrational Properties of TiS_2, ZrS_2, and HfS_2: Periodic Trends Studied by Dispersion-Corrected Hybrid Density Functional Methods

Nina Glebko, Irina Aleksandrova, Girish C. Tewari, Tripurari S. Tripathi, Maarit Karppinen, and Antti J. Karttunen*

Department of Chemistry and Materials Science, Aalto University, P.O. Box 16100, FI-00076 Aalto, Finland

Supporting Information

ABSTRACT: The electronic and vibrational properties of TiS_2, ZrS_2, and HfS_2 have been studied using dispersion-corrected hybrid density functional methods. The periodic trends in electronic band structures, electronic transport coefficients, IR and Raman spectra, and phonon dispersion relations were investigated. Comparison to the available experimental data shows that the applied DFT methodology is suitable for the investigation of the layered transition metal dichalcogenide materials with weak interlayer van der Waals interactions. The choice of damping function in the D3 dispersion correction proved to have a surprisingly large effect. Systematic investigation of the periodic trends within group 4 disulfides reveals that TiS_2 shows many differences to ZrS_2 and HfS_2 due to the more covalent M−S bonding in TiS_2. ZrS_2 and HfS_2 mainly show differences for properties where the atomic mass plays a role. All three compounds show similar Seebeck coefficients but clear differences in the relative electrical conductivity of cross- and in-plane directions. The transport and vibrational properties of thin TiS_2 single crystals were also investigated experimentally.

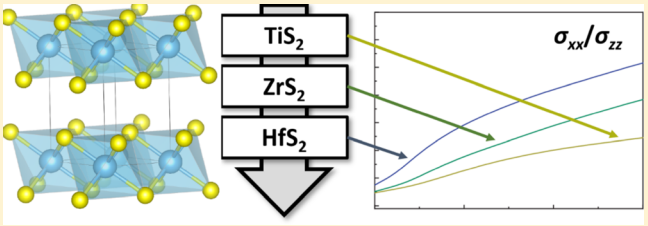

INTRODUCTION

Group 4 transition metal disulfides TiS_2, ZrS_2, and HfS_2 adopt a trigonal, layered CdI_2-type structure (Figure 1, space group $P\bar{3}m1$). The intralayer metal−chalcogen bonding in the *ab*-plane (in-plane) is ionic/covalent, while the layers are stacked via weak van der Waals interactions along the *c* axis (cross-plane). Each metal atom is surrounded by six sulfur atoms in trigonal prismatic coordination, and each S atom is connected to three metal atoms. The fact that TiS_2, ZrS_2, and HfS_2 possess similar CdI_2-type structure opens the possibility for systematic computational studies into their periodic, groupwise trends. The Hf atom is of rather similar size as Zr due to lanthanoid contraction, and Zr and Hf often show rather similar electronic properties. However, the two elements show a clear mass difference, which can be expected to affect the periodic trends of vibrational and thermal properties of Zr and Hf compounds.

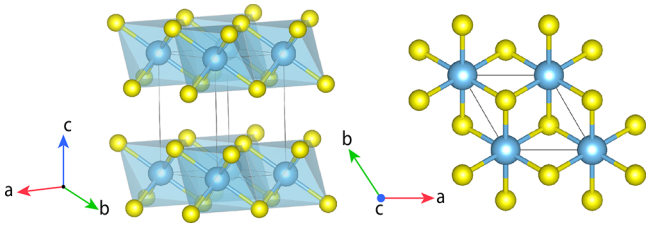

Figure 1. Crystal structure of the studied MS_2 compounds (M = Ti, Zr, Hf). Left: Side view. Right: top view. Blue: M, yellow: S.

The layered structure of group 4 transition metal disulfides allows an immense number of possible intercalation reactions, where guest atoms or molecules are accommodated in the interlayer space. The intercalation reactions make it possible to tune the properties of the parent MS_2 lattice, resulting for example in lower thermal conductivity and higher thermoelectric efficiency.

Thermoelectric materials can be used to produce electrical energy from temperature gradients that can be found for example from industrial settings, microelectronics, or even the human body/ambient air interface. The growing need to harvest low-grade waste heat has stimulated studies toward cheaper and environmentally more friendly thermoelectric (TE) materials that could be used to substitute most commonly used TE materials such as Bi_2Te_3 or PbTe.[1,2] Combining experimental synthesis and engineering of TE materials with *ab initio* quantum chemical methods with predictive power provides the means for rational design of novel TE materials.[3]

Received: August 20, 2018
Revised: November 6, 2018
Published: November 6, 2018

DOI: 10.1021/acs.jpcc.8b08099
J. Phys. Chem. C 2018, 122, 26835−26844

The performance of thermoelectric materials is evaluated by dimensionless figure of merit ZT, which can be expressed by eq 1

$$ZT = S^2\sigma T/\kappa \quad (1)$$

where S is Seebeck coefficient (thermopower); σ is electrical conductivity; κ is thermal conductivity; and T is the temperature. κ can be considered as the sum of electronic contribution (κ_{el}) and phonon contribution (κ_l):

$$\kappa = \kappa_{el} + \kappa_l \quad (2)$$

In insulators and semiconductors, κ_l typically dominates over κ_{el}.

Intercalated group 4 transition metal disulfides are potential TE materials due to the performance improvements arising from the intercalation.[4−8] For example, intercalating TiS_2 by Cu results in significant improvement in thermoelectric efficiency and also decreases the anisotropy of ZT in the in-plane and cross-plane directions.[9] In fact, TiS_2 is typically synthesized in nonstoichiometric form $Ti_{1+x}S_2$, where the excess Ti atoms are intercalated between the TiS_2 sheets.[10] On the other hand, intercalation by organic molecules has been shown to lead to major reduction of lattice thermal conductivity and improvement of ZT in a number of studies.[11,12] Furthermore, it is possible to derive superlattices such as $(SnS)_{1.2}(TiS_2)_2$ by intercalating the TiS_2 lattice by layers from other layered materials such as SnS. This approach also reduces the lattice thermal conductivity significantly, resulting in improved ZT.[13]

The fundamental electronic properties of the group 4 disulfides have been investigated in a number of publications, and all of them are known to be n-type semiconductors. For the band gap of TiS_2, there are several conflicting experimental reports. In a number of papers, TiS_2 has been described as a semiconductor with band gap varying from 0.2 to 1.5 eV,[14−18] while few other studies describe it as a semimetal.[19−21] The discrepancy can be explained by taking into account structural defects and the well-known tendency of TiS_2 to be non-stoichiometric.[22] Possibly due to the difficulties in synthesis of good quality single crystals, there are fewer experimental works on the band gap of ZrS_2 and HfS_2. However, ZrS_2 and HfS_2 are generally accepted as semiconductors with band gap range of 1.68−1.78 eV and 1.96−2.85 eV, respectively.[16,23,24]

The majority of previous computational studies on group 4 transition metal disulfides has focused on the properties of TiS_2. Allan et al. investigated the effect of pressure on the crystal structure and electronic properties of TiS_2, utilizing density functional theory in local density approximation (DFT-LDA).[25] According to their results, TiS_2 is a semiconductor with a band gap of about 1.9 eV at ambient conditions. Fang et al. carried out DFT-LDA calculations for TiS_2 and $TiSe_2$, reporting that single-layered TiS_2 is a semiconductor with about 1 eV band gap, which then decreases as the number of monolayers increases and eventually turns to a semimetal in bulk.[26] Reshak et al. studied the electronic and optical properties of MX_2 (M = Ti, Zr; X = S, Se, Te) with DFT-LDA,[27,28] concluding that TiS_2 and ZrS_2 are semimetallic and semiconducting, respectively (1.4 eV band gap for ZrS_2). In two other studies, Hubbard U correction was used (GGA+U and LDA+U) to study the electronic[29] and vibrational properties[30] of TiS_2. In both studies, TiS_2 was found to be a semiconductor with a band gap of 1 eV.

To our knowledge, the periodic trends of electronic and vibrational properties of group 4 transition metal disulfides TiS_2, ZrS_2, and HfS_2 have not been examined previously. Jiang investigated the electronic and vibrational properties of ZrS_2 and HfS_2 with various local and semilocal DFT methods and many-body perturbation theory (GW approximation).[31] The band gaps calculated within the GW approximation were generally in good agreement with the experiment, showing an overestimation of 0.1−0.3 eV depending on the experimental reference. Yumnam et al. studied the electronic and thermal transport properties of ZrS_2 and HfS_2 using GGA-PBE and modified Becke−Johnson TB-mBJ functionals.[32] They found ZrS_2 and HfS_2 to be semiconductors with band gaps of 1.3 and 1.7 eV, respectively, being about 0.26−0.4 eV smaller than the experimental values.

Recently, the vibrational and dielectric properties of various transition metal dichalcogenides including TiS_2 and ZrS_2 have been studied with DFT and DFPT by Pike et al.[33] The main computational tool in the work was the DFT-PBE functional, combined with Grimme's dispersion correction (DFT-D3). The work of Pike et al. clearly highlights the importance of using a computational method that can properly describe the weak interlayer van der Waals interactions. The data obtained with PBE-D3 were reported as the most accurate with respect to the experiment, and the dispersion correction had an effect on both the cross-plane c-direction and the ab plane.

Here we investigate the periodic trends of the electronic, vibrational, and thermoelectric properties of group 4 transition metal disulfides TiS_2, ZrS_2, and HfS_2. We apply dispersion-corrected hybrid density functional methods and Gaussian-type local basis sets to describe both the crystal structure and electronic structure of all three group 4 disulfides. Finding a level of theory that can consistently reproduce the experimentally observed periodic trends is also a prerequisite for further computational studies into the intercalation of group 4 transition metal disulfides.

COMPUTATIONAL DETAILS

The DFT calculations were carried out with the CRYSTAL14[34] program using the PBE0[35] hybrid density functional. The results discussed in the main paper have been obtained with a Gaussian-type triple-ζ-valence+polarization basis set (TZVP) derived from the molecular Karlsruhe basis sets.[36] Comparisons to smaller split-valence+polarization (SVP) and larger TZVPP basis sets as well as detailed basis set listings are included as Supporting Information. The weak interlayer interactions were taken into account using Grimme's empirical D3 dispersion correction.[37] The influence of the damping function in the D3 correction was evaluated by calculating the lattice parameters with both zero damping (ZD) and Becke−Jones (BJ) damping.[38] After initial benchmark calculations, all production calculations were carried out at the DFT-PBE0-D3(ZD)/TZVP level of theory.

The structures of the studied compounds were fully optimized within the $P\bar{3}m1$ space group. Default optimization convergence criteria and DFT integration grid of CRYSTAL14 were applied. Based on the results of convergence tests, the reciprocal space was sampled using a Monkhorst−Pack-type 8 × 8 × 6 k-mesh.[39] All Brillouin zone paths for electronic band structures and phonon dispersions were taken from ref 40. The majority of the calculations was conducted using very tight Coulomb and exchange integral tolerance factors of 8, 8, 8, 8, and 16 (TOLINTEG). In the case of TiS_2 phonon dispersion

DOI: 10.1021/acs.jpcc.8b08099
J. Phys. Chem. C 2018, 122, 26835−26844

calculations, even tighter values of 9, 9, 9, 9, and 18 were needed to avoid numerical inaccuracies in the force constant calculation.

The vibrational frequencies at the Γ point were obtained within the harmonic approximation by calculating the numerical second derivatives of the potential energy using the scheme implemented in CRYSTAL.[41,42] IR and Raman intensities for simulating spectra were obtained with the Coupled Perturbed Hartree−Fock method implemented in CRYSTAL.[43,44] The IR absorbances are reported in units of km mol^{-1}, while the Raman intensities are in arbitrary units and normalized to the strongest intensity peak. The IR spectra were broadened by using Lorentzian line shape and fwhm of 16 cm^{-1}. The Raman spectra were broadened using pseudo-Voigt peak profile (50:50 Lorenzian:Gaussian) and fwhm of 16 cm^{-1}.

Phonon dispersion calculations were carried out within the harmonic approximation using Phonopy code, which utilizes supercell approach coupled with finite displacement method.[45,46] In all vibrational frequency and phonon calculations, the convergence criterion of the total energy was set to 10^{-10} a.u. to obtain accurate forces. The second order force constants were calculated for ZrS_2 and HfS_2 using 3 × 3 × 2 supercell and atomic displacement amplitude of 0.03 Å. TiS_2 phonon dispersion calculation required a larger 5 × 5 × 3 supercell (see Supporting Information for convergence tests). Additionally, a diagonal finite displacement with an amplitude of 0.09 Å had to be used. Such relatively large atomic displacements have been utilized previously for Mo- and W-based layered dichalcogenides and proven to be reasonable.[47] According to our benchmarks presented in the Supporting Information, the displacement amplitude does not have a significant effect on overall phonon dispersion picture but improves the numerical stability in the case of TiS_2. Nonanalytical correction at $\mathbf{q} \rightarrow 0$ was taken into account by using the formulation of Wang et al.[48]

The Seebeck coefficient and electrical conductivity with respect to the relaxation time were calculated with the BoltzTraP code[49] which is based on Fourier expansion of electron band energies combined with Boltzmann transport theory. The transport coefficients are solved within the constant relaxation time and rigid band approximations. CRYSTAL was used to calculate the wave functions for BoltzTraP. For the transport coefficient calculations, we used a dense k-mesh of 58 × 58 × 29.

EXPERIMENTAL SECTION

To obtain experimental data on the transport and vibrational properties of TiS_2, we synthesized single crystals via the vapor transport method using iodine as the transport agent (5 mg/cm^3).[50,51] The original procedure reported in the literature was slightly modified in order to achieve higher purity. The quartz ampule used in the synthesis was carefully cleaned and evacuated within a Schlenk line to prevent oxidation reactions. Stoichiometric amounts of Ti and S powders were mixed in the reaction ampule, which was sealed and placed in the furnace at 650 °C for 15 h with heating rate of 1.25 °C/min. After cooling, the reaction ampule was relocated to a tube furnace with a linear temperature gradient from 800 to 900 °C and heated for 3 days. Eventually, yellow-brownish thin crystals with metallic luster were obtained. The Raman spectrum of TiS_2 was recorded with a Horiba LabRAM HR Raman microscope system using wavelength of 632.8 nm. The in-plane Seebeck coefficient (S), DC electrical resistivity (ρ), and Hall coefficient (R_H) together with carrier concentration (n) were measured using the Quantum Design Physical Property Measurement System.

RESULTS

Structural Parameters. As discussed above, TiS_2, ZrS_2, and HfS_2 possess an anisotropic, layered crystal structure where the cross-plane c-parameter of the unit cell is governed by weak van der Waals interactions and the a parameter is determined by the intralayer M−S structure and bonding. To evaluate the importance of dispersion correction, we conducted geometry optimizations using (a) plain PBE0 with no dispersion correction, (b) PBE0-D3 with Becke−Jones damping, and (c) PBE0-D3 with zero damping (Table 1).

Table 1. DFT-Optimized and Experimental[52,53] Lattice Constants a and c (in Å) for TiS_2, ZrS_2, and HfS_2[a]

param.	TiS_2	ZrS_2	HfS_2
	PBE0		
a	3.41 (+0.0%)	3.68 (+0.5%)	3.68 (+1.3%)
c	6.22 (+9.0%)	6.43 (+10.5%)	6.67 (+14.2%)
	PBE0-D3(BJ)		
a	3.36 (−1.4%)	3.63 (−0.8%)	3.64 (+0.1%)
c	5.51 (−3.3%)	5.62 (−3.4%)	5.65 (−3.1%)
	PBE0-D3(ZD)		
a	3.40 (−0.4%)	3.66 (−0.1%)	3.66 (+0.6%)
c	5.67 (−0.7%)	5.73 (−1.5%)	5.73 (−1.8%)
	Experimental Data		
a	3.41	3.66	3.64
c	5.71	5.81	5.84

[a]The numbers in parentheses show the deviation from experimental values.

Using plain PBE0 with no dispersion corrections resulted in a strong overestimation of the c parameter compared to the experimental values. The error in the predicted c parameter ranged from 9.0% to 14.2%, with Ti showing the smallest error and Hf the largest. We also tested the performance of a plain GGA-PBE functional with no dispersion corrections. The predicted lattice constants are rather similar to plain PBE0, with large errors in the c parameter. Furthermore, when using PBE, TiS_2 becomes metallic, and the band gap of ZrS_2 and HS_2 is two times smaller compared to the PBE0 results. Consequently, PBE was not used in any further calculations (the PBE benchmark results are listed in the Supporting Information).

The structural parameters shown in Table 1 illustrate how the DFT-PBE0-D3(BJ) gives too strong interlayer interaction and results in underestimated c parameter. The DFT-PBE0-D3(ZD) approach shows smaller deviations in comparison to the experimental values of the c parameter. Related to our findings here, Pike et al. have recently compared DFT-PBE-D3(ZD) and DFT-PBE-D3(BJ) for several layered transition metal dichalcogenides and reported that DFT-PBE-D3(ZD) gave better agreement with experimental low-energy phonon branches.[33] Based on our geometry optimization benchmarks and additional basis set convergence tests described in the Supporting Information, we chose DFT-PBE0-D3(ZD)/TZVP level of theory for studying the properties of TiS_2, ZrS_2, and HfS_2.

DOI: 10.1021/acs.jpcc.8b08099
J. Phys. Chem. C 2018, 122, 26835−26844

In addition to the structural parameters, we also investigated the interlayer binding energies of TiS_2, ZrS_2, and HfS_2. The interlayer binding energy E_b is defined here as $E_b = E(\text{bulk}) - E(\text{monolayer})$. The structure of each MS_2 monolayer was fully relaxed. The interlayer binding energies for TiS_2, ZrS_2, and HfS_2 are 29.4, 28.9, and 28.2 kJ/mol, respectively. Taking the surface area of each monolayer into account, the E_b values become 26.5, 22.4, and 21.8 meV/Å^2. This compares very well with the E_b values of 28.6, 24.5, and 24.2 meV/Å^2 obtained by Björkman et al. using the Vydrov–van Voorhis (VV10) density functional method. The trend shows that the monolayers are slightly more strongly bound in the case of TiS_2 in comparison to ZrS_2 and HfS_2, where the interlayer binding energies are very similar.[54]

Band Structures. The electronic band structures of TiS_2, ZrS_2, and HfS_2 are illustrated in Figure 2. The general features of the band structure are rather similar, and all three materials are semiconductors. The valence bands are dominated by sulfur 3p orbitals, whereas the conduction bands are dominated by transition metal d orbitals. When moving from Ti to Hf, the conduction bands increase in energy, and the band gap increases for $TiS_2 \rightarrow ZrS_2 \rightarrow HfS_2$ as 1.4 eV → 2.7 eV → 3.3 eV, respectively. As discussed in the Introduction, the available experimental data vary as 0.2–1.5 eV → 1.68–1.78 eV → 1.96–2.85 eV, the largest band gap values corresponding to the most stoichiometric phases. The DFT-PBE0 and gaps thus seem to be slightly overestimated in comparison to the available experimental values, in particular for ZrS_2. Unfortunately, accurate estimates of the sample stoichiometry are not available in the case of ZrS_2.

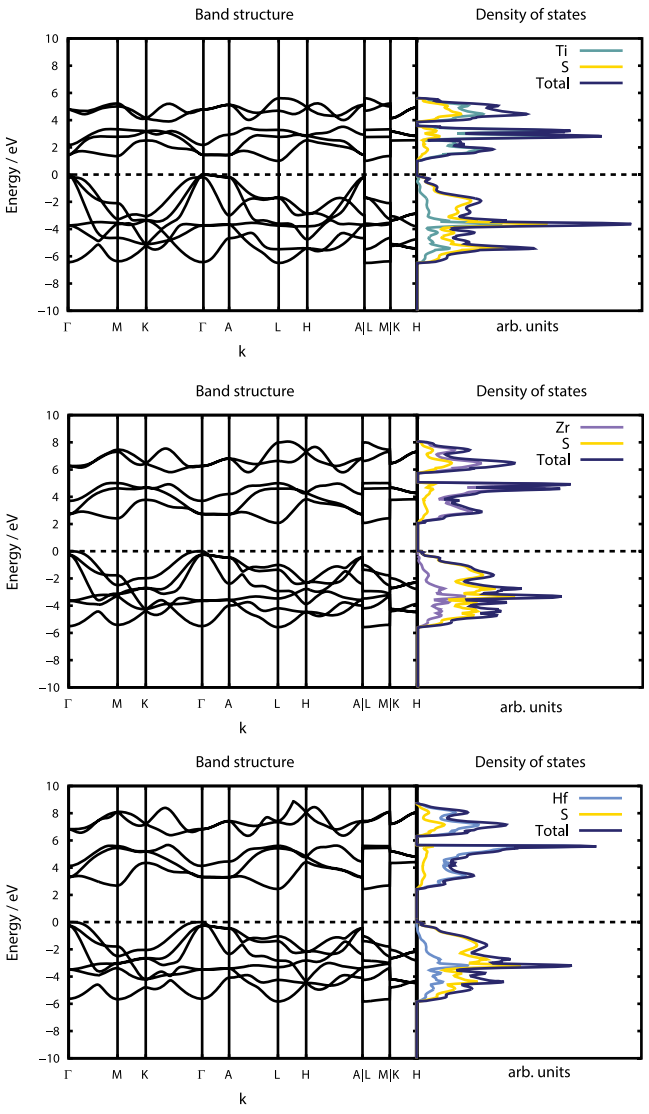

Figure 2. Band structure and density of states (DOS) at the DFT-PBE0-D3(ZD)/TZVP level of theory: (a) TiS_2; (b) ZrS_2; (c) HfS_2. The top of the valence bands is at 0 eV.

Population Analyses. We investigated the nature of the intralayer M–S bonding by carrying out Mulliken population analysis. The partial atomic charges are $Ti^{+0.48}S_2^{-0.24}$, $Zr^{+0.93}S_2^{-0.47}$, and $Hf^{+0.94}S_2^{-0.47}$ which suggests more ionic bonding for ZrS_2 and HfS_2 in comparison to TiS_2. The Mulliken bond population of the M–S bond behaves as $ZrS_2 \approx HfS_2 < TiS_2$ with values of 0.18, 0.18, and 0.20 e^-, respectively. In conclusion, the M–S bonding in TiS_2 can be considered to possess the most covalent character of the studied three materials. This is also in agreement with the trend of the Pauling electronegativities (1.54, 1.33, and 1.3 for Ti, Zr, and Hf, respectively).

Electronic Transport Coefficients. As the group 4 disulfides are prospective thermoelectric materials, we investigated their Seebeck coefficient (thermopower) and electrical conductivity at 300 K. The experimental transport coefficients are usually available only in the *ab*-plane because the thin single crystals make it difficult to determine the cross-plane transport coefficients. All group 4 disulfides are known to be n-type semiconductors, but we have investigated the Seebeck coefficient for both n- and p-type doping and for both in-plane and cross-plane. Figure 3 illustrates the *ab*-plane Seebeck coefficient S_{xx} for n-type TiS_2, ZrS_2, and HfS_2 within relevant doping levels. There is practically no difference in the n-type S_{xx} values between the three materials. This is reasonable as the Seebeck coefficient arises from the electronic band structure, and the band structures in Figure 2 show how similar the conduction bands of the three materials are. Concerning the anisotropy of the Seebeck coefficient for n-doping, the S_{xx} coefficient is larger than the S_{zz} coefficient in the studied doping range. At an experimentally relevant carrier concentration of of 2.5×10^{20}, the S_{xx} coefficient is larger by about 10, 15, and 20 μV/K for TiS_2, ZrS_2, and HfS_2, respectively. In relative terms, this means about 10% anisotropy for TiS_2 at 300 K. The anisotropy is expected to arise from the different in-plane and cross-plane contributions to the electronic density of states at this doping level. However, due to the relatively small anisotropy, this is not easy to quantify from the band structure and DOS plots. The anisotropy of S has been observed in previous experimental studies for textured polycrystalline TiS_2,[9,13] which showed S_{xx} to be larger than S_{zz}. In the case of p-type doping, the overall $|S_{xx}|$ values are smaller than for n-type doping, and we did not pursue more detailed investigation in this direction.

The transport properties of TiS_2 in both single-crystal and polycrystalline form have been studied extensively.[5,8] Often the experimental results have been presented as a function of temperature instead of doping level,[11,55] but the effect of the carrier concentration has also been investigated in a number of studies.[4,5,7,8,10] Here we focus on the experimental results obtained for TiS_2 single crystals at 300 K. The lack of experimental transport data for ZrS_2 and HfS_2 prevents us from presenting any comparisons for them.

DOI: 10.1021/acs.jpcc.8b08099
J. Phys. Chem. C 2018, 122, 26835–26844

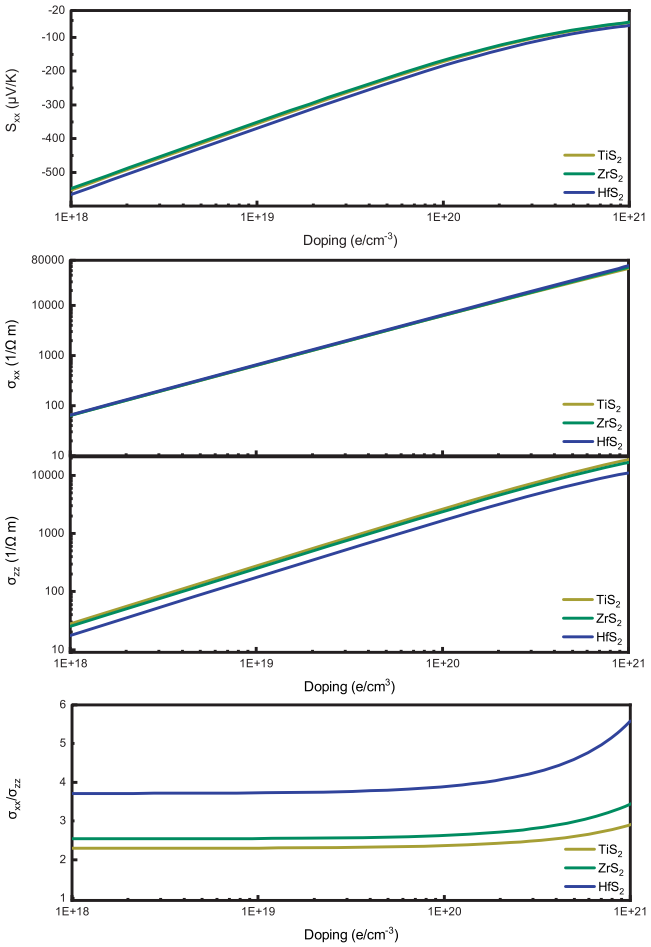

Figure 3. Top: Seebeck coefficient for n-type doped TiS_2, ZrS_2, and HfS_2 in *ab*-plane (S_{xx}) direction. Middle: Electrical conductivity in *ab*-plane (σ_{xx}) and cross-plane direction (σ_{zz}) with constant electronic relaxation time of 10^{-15} s. Bottom: Ratio of *ab*-plane and cross-plane electrical conductivity.

The pioneering study of Imai et al.[55] reported the in-plane Seebeck coefficient of −251 μV/K with carrier concentration of 2.8×10^{20} cm^{-3}. Later, Koumoto et al.[11] reported an in-plane Seebeck coefficient of −171 μV/K with doping level of 3.4×10^{20} cm^{-3}. The fact that 20% higher charge carrier concentration results in a clearly lower Seebeck coefficient can be explained by nonstoichiometry effect: the excess of Ti atoms inside the interlayer space leads to higher carrier concentration and shifting of the Fermi level toward 3d metal bands, decreasing the Seebeck coefficient. Daou et al. recently investigated the in-plane transport properties of TiS_2 single crystals,[6] reporting Seebeck coefficient of −97 μV/K and carrier concentration of 1.8×10^{21} cm^{-3}. The TiS_2 single crystals synthesized in this study show a carrier concentration of 1.3×10^{21} cm^{-3}, fairly close to the value reported by Daou et al. For this carrier concentration, we measured an in-plane Seebeck coefficient of −106 μV/K. Our $|S_{xx}|$ is slightly larger than for Daou et al., which is fully understandable due to the lower carrier concentration in our sample. Considering our predicted values, a doping level of 1.3×10^{21} cm^{-3} results in S_{xx} of −50 μV/K, and a lower doping level of 2.6×10^{20} cm^{-3} produces S_{xx} of −103 μV/K. The predicted $|S_{xx}|$ is thus underestimated in comparison to the experimental values. The agreement could perhaps be improved by using a higher level of theory, but it is not easy to improve further from the hybrid DFT methods applied here. Another important reason for the underestimation may be the rigid band approximation used in the transport calculations: the effect of doping is considered to just cause a rigid shift of the Fermi level in the band structure, while in reality the rather high carrier concentrations typically observed in TiS_2 may break the rigid band approximation. Despite the underestimation of the absolute values of S_{xx}, the trend of S_{xx} vs carrier concentration appears to be reproduced rather well. When the carrier concentration is increased first from 2.8×10^{20} to 1.3×10^{21} cm^{-3} and then further to 1.8×10^{21} cm^{-3}, S_{xx} first decreases by 53% and then by 11%. In the experimental studies discussed above, the corresponding decrease in S_{xx} was 57% and 8%.

Concerning the electrical conductivity, BoltzTraP can presently calculate it only with respect to the electron relaxation time τ, which is assumed to be direction-independent.[49] In many computational studies of thermoelectric properties, τ is set to about 10^{-14} s,[56] but this may lead to overestimation of the TE performance. We have used here shorter electronic relaxation time of 10^{-15} s to avoid any overestimation. The middle figure in Figure 3 shows the electrical conductivity trends for all studied systems. For TiS_2, Imai et al. and Daou et al. have reported resistivities of 1.7 and 0.8 mΩ cm, respectively.[6,55] For the TiS_2 single crystals synthesized in this study, we measured in-plane electrical resistivity of 1.3 mΩ cm. At the experimental carrier concentration of 1.3×10^{21} cm^{-3}, the electrical conductivity predicted here for TiS_2 is 91 480 S/m, which corresponds to 1.2 mΩ cm.

The electrical conductivity values predicted for the *ab*-plane and cross-plane directions are clearly different. To investigate the anisotropy in detail, we have plotted σ_{xx}/σ_{zz} in the bottom part of Figure 3. The anisotropy increases with increasing carrier concentration and also when moving from TiS_2 to HfS_2. Considering the layered structure of the studied materials, it is not surprising that the *ab*-plane electrical conductivity is significantly larger than in the cross-plane direction. However, the anisotropy observed here is significantly smaller in comparison to the 750-fold anisotropy ratio reported by Imai et al. for TiS_2 single crystal at 300 K.[55] A possible reason for this discrepancy could be the constant relaxation time approximation applied in our calculation, which means that we assume similar electronic relaxation time for the *ab*-plane and cross-plane direction. Interestingly, in textured ceramic TiS_2 samples, the anisotropy ratio has been shown to be about 2.[4]

IR/Raman Spectra. Vibrational properties of a material play a key role in understanding various thermodynamic and transport properties of solids, including lattice thermal conductivity.[57] The phonon modes at the Γ-point of the first Brillouin zone can be examined by Raman and IR spectroscopies. The primitive cell of TiS_2, ZrS_2, and HfS_2 consists of two chalcogen atoms and one metal atom with trigonal prismatic coordination, resulting in three acoustic modes and six optical modes, the latter of which split in three g-modes and three u-modes due to the presence of inversion center:

$$\Gamma = A_{1g} + E_g + 2A_{2u} + 2E_u \quad (3)$$

A_{1g} and E_g modes are Raman active, while A_{2u} and E_u modes are IR active. One A_{2u} mode and one $2E_u$ mode correspond to the acoustic modes. The A-modes represent the atomic displacement along the Cartesian *z* axis (out-of-plane

DOI: 10.1021/acs.jpcc.8b08099
J. Phys. Chem. C 2018, 122, 26835−26844

modes), and the doubly degenerate E-modes represent atomic displacements along both x and y axes (in-plane modes). The atomic displacements are illustrated in Figure 4, and the

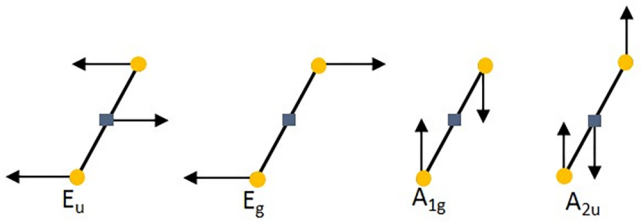

Figure 4. Atomic displacements in the IR- and Raman-active modes of TiS_2, ZrS_2, and HfS_2. Blue square and yellow circles represent metal and sulfur atoms, respectively.

Table 2. Calculated Vibrational Frequencies of the IR and Raman Active Optical Modes in TiS_2, ZrS_2, and HfS_2 (cm^{-1} units)[a]

mode	TiS_2	ZrS_2	HfS_2
E_u	115 (−35.8%)	168 (−6.4%)	169 (+1.6%)
E_g	258 (+9.8%)	263 (+4.7%)	270 (+3.2%)
A_{1g}	361 (+7.8%)	340 (−2.7%)	346 (+2.6%)
A_{2u}	408 (+9.8%)	346 (−1.2%)	319 (−1.9%)

[a]The values in parentheses show the difference in the experimental spectra.[60,61]

calculated vibrational frequencies are summarized in Table 2. In the case of ZrS_2 and HfS_2, the calculated vibrational frequencies are in good agreement with the experimental values. For TiS_2, the differences between the theory and experiment are larger, especially for the lowest energy E_u mode. We do not have any conclusive explanation why the E_u mode shows such a large difference, but it could be related to the high tendency for nonstoichiometry in TiS_2 single crystals. Previous studies of nonstoichiometric TiS_2 have mostly focused on its effect on the electronic properties and less on the vibrational properties. Friend et al. did investigate the effect of excess Ti atoms for the high energy A_{1g} optical mode, observing a small shift toward smaller wavenumbers caused by increasing carrier concentration, along with broadening of the peak toward higher energy (appearance of a shoulder).[22,58] Sandoval et al. suggested the broadening to arise from overtone and/or summation processes.[59]

We also calculated the IR and Raman intensities, and the simulated IR and Raman spectra for TiS_2, ZrS_2, and HfS_2 are presented in Figures 5 and 6. Looking at the periodic trends in the simulated spectra, we can observe that the energy gap between the optical modes decreases when moving from Ti to Hf, and the energy gap for TiS_2 is clearly larger than for ZrS_2 and HfS_2. In the Raman spectra, the intensity of the in-plane E_g mode is about three times smaller than that for cross-plane A_{1g} mode. This is in line with the experimental Raman spectra reported for ZrS_2 and HfS_2.[61] For the IR-active modes, the situation is reversed, and the in-plane E_u mode has a much larger absorbance in comparison to the cross-plane A_{2u} mode.

We also have compared the predicted Raman spectra of TiS_2 with the experimental Raman spectrum measured for the single crystals prepared for this work (Figure 7). To facilitate comparisons with the experiment, the calculated intensities of

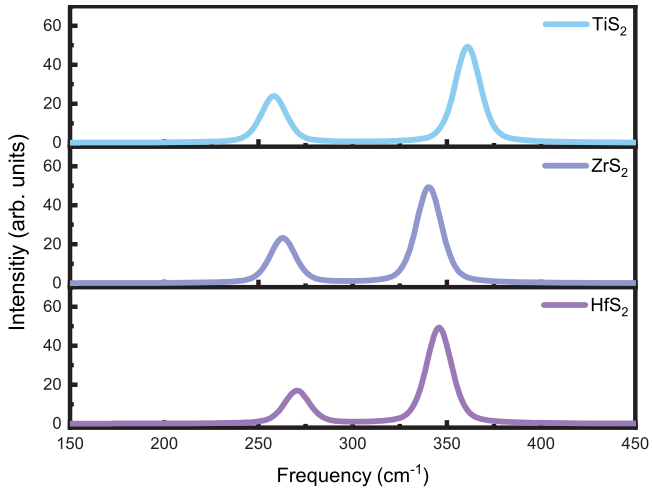

Figure 5. Calculated Raman spectra for TiS_2, ZrS_2, and HfS_2.

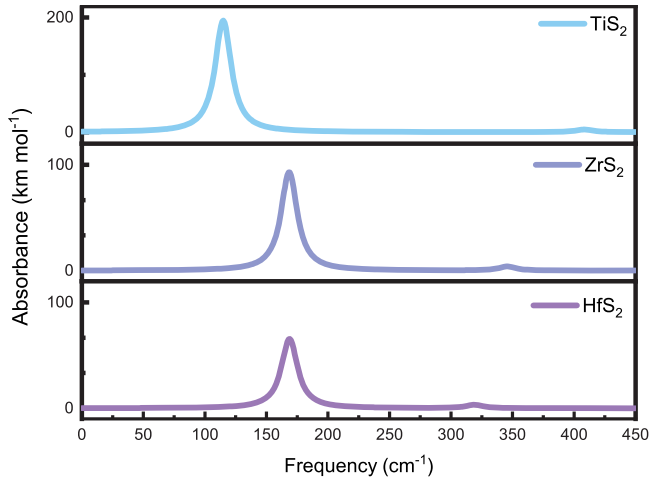

Figure 6. Calculated IR spectra for TiS_2, ZrS_2, and HfS_2. Note that the y-axis scale for TiS_2 is different.

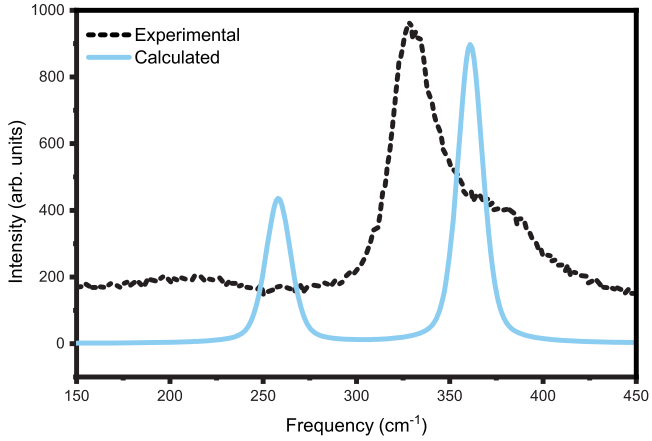

Figure 7. Simulated and experimental Raman spectrum of TiS_2 (both spectra from this work).

TiS_2 were scaled by a factor of 18.18. Similar to our TiS_2 Raman spectrum in Figure 7, other groups have reported broadening and the appearance of a shoulder for the A_{1g} Raman peak for all three group 4 disulfides.[61−63] Unlike for TiS_2, the shoulder is significantly smaller for ZrS_2 and HfS_2 and

DOI: 10.1021/acs.jpcc.8b08099
J. Phys. Chem. C 2018, 122, 26835−26844

appears on the left side of the A_{1g} peak. Earlier studies have attributed the shoulder to the coupling of IR and Raman active modes due to a resonance effect or, as mentioned above, to nonstoichiometry.[22,61,63,64] More recent studies have suggested nonharmonic effects such as the emission of a low-energy acoustic phonon by the optical phonon as the reason for the broadening[62]

For the IR active E_u and A_{2u} modes, the splitting in longitudinal optical (LO) and transverse optical (TO) modes can also be investigated. The LO−TO splitting has been observed experimentally, primarily for the E_u mode, but has not been examined systematically computationally.[65,66] We have calculated the LO−TO splitting of the E_u and A_{2u} modes and summarized the results in Table 3 together with the

Table 3. Calculated and Experimental[61,63,66] LO−TO Splitting for TiS_2, ZrS_2, and HfS_2 (cm^{-1} Units)

mode	TiS_2	ZrS_2	HfS_2
E_u (DFT)	276	199	165
E_u (exptl)	248	170	155
A_{2u} (DFT)	20	22	20

available experimental data. The predicted LO−TO splittings for the E_u mode are in a reasonable agreement with the experimental data. The LO−TO splitting is much larger for the low-energy E_u mode in comparison to the A_{2u} mode.

To predict the LO−TO splittings, high frequency dielectric constants (ε_∞) and Born effective charges were also calculated. Direct comparisons of the dielectric constants with experiments are complicated by the wide range of experimental data reported. For example, in the case of TiS_2, ε_∞ varies in the range 13.7−19.8.[20,67] The overall trend of decreasing ε_∞ for TiS_2 (15.7) → ZrS_2 (8.3) → HfS_2 (7.6) was reproduced in our calculations.

Phonon Dispersions. The calculated phonon dispersion relations and phonon density of states (DOS) for TiS_2, ZrS_2, and HfS_2 are illustrated in Figure 8. The group velocity of the longitudinal acoustic (LA) mode in the Γ−*A* direction is rather similar for TiS_2 (3.7 km/s) and ZrS_2 (3.4 km/s) and somewhat smaller in HfS_2 (2.7 km/s). This direction corresponds to the cross-plane direction in the real space and is governed by the weak van der Waals interactions. In the Γ−*M* direction the group velocities of the LA mode are clearly higher in comparison to the Γ−*A* direction. At the same time, the group velocities clearly decrease when moving from TiS_2 (6.5 km/s) to ZrS_2 (5.1 km/s) and HfS_2 (4.2 km/s). This direction corresponds to the *ab*-plane in the real space and corresponds to intralayer M−S bonding. For TiS_2, there is also some experimental data available on the longitudinal (5.3 km/s) and transverse (3.3 and 2.8 km/s) sound velocities.[13] The corresponding phonon group velocities from our calculations are 6.5, 4.4, and 2.4 km/s.

The decrease of phonon energy and group velocity when moving from TiS_2 to HfS_2 suggests that the M−S bonding in TiS_2 is more covalent than in ZrS_2 and HfS_2, in agreement with the population analysis and Pauling electronegativity differences discussed above. At the same time, the phonon gap between acoustic and optical phonons increases when moving from TiS_2 to HfS_2, showing clear difference also between Zr and Hf. The appearance of a phonon band gap between the acoustic and optical modes may have an effect on the phonon scattering processes and hence the lattice thermal conductivity

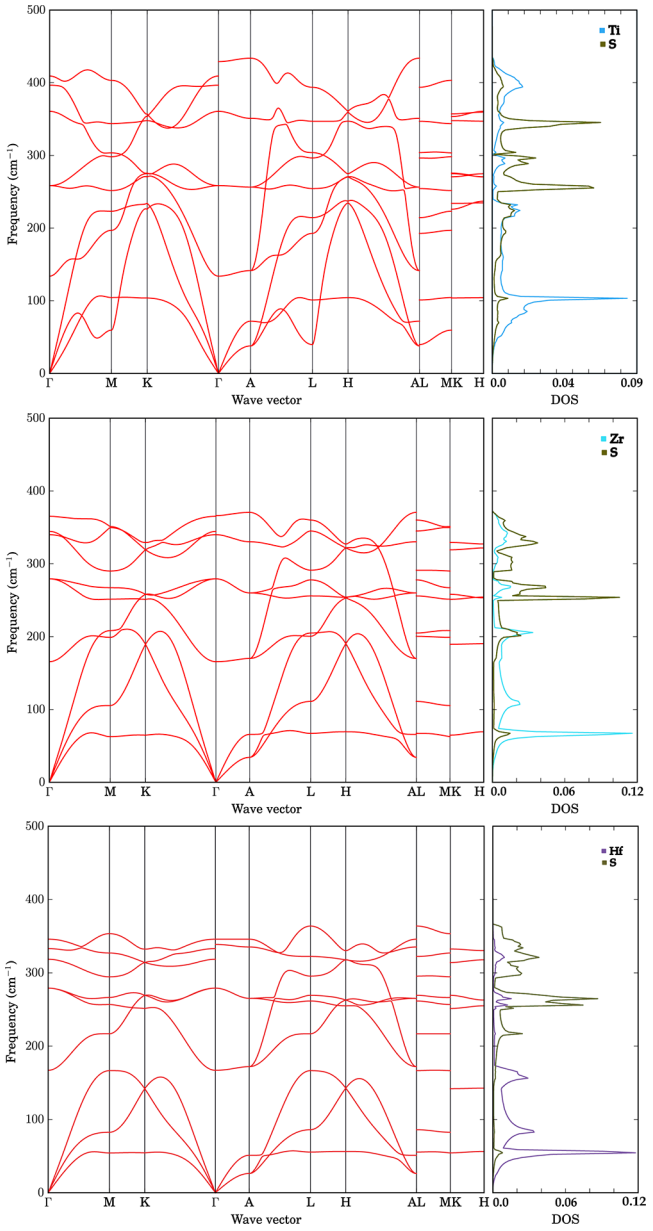

Figure 8. Phonon dispersion relations and phonon density of states (in arbitrary units) for TiS_2 (top), ZrS_2 (middle), and HfS_2 (bottom). Nonanalytical correction at $\mathbf{q} \rightarrow 0$ has been taken into account in the phonon dispersion relations.[48] Note that the DOS scale is different for all three materials.

of a material. From the phonon DOS we can conclude that acoustic phonons are mostly dominated by displacements of the transition metal atoms, while displacements of the sulfur atoms dominate the high-energy optical phonons. In addition to the phonon dispersion relations, predicting the lattice thermal conductivity κ_l and total thermoelectric figure of merit *ZT* would require the calculation of third-order (anharmonic) force constants.

The TiS_2 phonon dispersion plot shows a soft phonon mode between Γ and *M* wave vectors. The mode softening has been suggested to be due to a charge density wave distortion (CDW), that is, electron density modulation caused by a disruption in the periodic lattice.[30,68,69] CDWs are known to occur for metallic low-dimensional solids at low temperatures. However, ideal TiS_2 is semiconducting, and it is normally not

DOI: 10.1021/acs.jpcc.8b08099
J. Phys. Chem. C 2018, 122, 26835−26844

classified as a CDW material.[70,71] For instance, Van Bakel et al. described TiS_2 as a "dirty" small band gap semiconductor which does not show any significant CDW nature at any temperature.[72] In accordance with this, we do not observe CDW behavior since TiS_2 is a semiconductor in our calculations. Our benchmark calculations, discussed in the Supporting Information, show that a relatively large supercell is required to properly describe the TiS_2 acoustic phonon modes between $\Gamma-M$ and $A-L$ with the DFT-PBE0-D3 method.

CONCLUSION

We have investigated the periodic trends in the electronic and vibrational properties of group 4 disulfides TiS_2, ZrS_2, and HfS_2 using dispersion-corrected hybrid density functional methods. DFT-PBE0-D3(ZD)/TZVP level of theory performs well for a broad variety of electronic and vibrational properties without any system-dependent parametrization. The choice of the damping function for the D3 correction had a surprisingly large effect in the studied systems, the zero-damping approach giving better results in comparison to Becke−Johnson damping. Systematic investigation of the periodic trends within group 4 disulfides reveals that TiS_2 shows many differences to ZrS_2 and HfS_2, the more covalent M−S bonding in TiS_2 clearly contributing to the differences. Concerning the thermolectric properties of the materials, all three compounds show similar Seebeck coefficients but clear differences in the relative electrical conductivity of cross- and in-plane directions. To fully understand the thermoelectric performance of the group 4 disulfides, the periodic trends of the lattice thermal conductivity must also be investigated. The DFT-PBE0-D3(ZD)/TZVP level of theory describes the group 4 disulfides with such accuracy that it appears to be a very reasonable computational approach for future studies on the lattice thermal conductivity. The phonon gap that arises between acoustic and optical phonons for Hf may have a noticeable effect on the phonon scattering processes and the thermal conductivity of HfS_2.

ASSOCIATED CONTENT

Supporting Information

The Supporting Information is available free of charge on the ACS Publications website at DOI: 10.1021/acs.jpcc.8b08099.

Additional computational results on the performance of GGA-PBE, basis set convergence tests, and phonon supercell convergence tests. Complete basis set details and the structural data in CRYSTAL input format (PDF)

AUTHOR INFORMATION

Corresponding Author

*E-mail: antti.j.karttunen@iki.fi.

ORCID

Maarit Karppinen: 0000-0003-1091-1169

Antti J. Karttunen: 0000-0003-4187-5447

Notes

The authors declare no competing financial interest.

ACKNOWLEDGMENTS

We would like to thank the Academy of Finland for funding (Mineral Resources and Material Substitution Programme, project 292431; project 294799) and CSC—the Finnish IT Center for Science for computational resources. The work was also supported by the RawMatTERS Finland Infrastructure (RAMI) based at Aalto University. We thank Prof. Kunihito Koumoto (Japan) for motivating discussions as well as Malte Sachs and Prof. Florian Kraus (Philipps-Universität Marburg) for guidance in the synthesis of TiS_2 single crystals.

REFERENCES

(1) Snyder, G. J.; Toberer, E. S. Complex Thermoelectric Materials. *Nat. Mater.* **2008**, *7*, 105−114.

(2) Tan, G.; Zhao, L.-D.; Kanatzidis, M. G. Rationally Designing High-Performance Bulk Thermoelectric Materials. *Chem. Rev.* **2016**, *116*, 12123−12149.

(3) Gorai, P.; Stevanovic, V.; Toberer, E. S. Computationally Guided Discovery of Thermoelectric Materials. *Nat. Rev. Mater.* **2017**, *2*, 17053.

(4) Guilmeau, E.; Bréard, Y.; Maignan, A. Transport and Thermoelectric Properties in Copper Intercalated TiS2 Chalcogenide. *Appl. Phys. Lett.* **2011**, *99*, 052107.

(5) Ohta, M.; Satoh, S.; Kuzuya, T.; Hirai, S.; Kunii, M.; Yamamoto, A. Thermoelectric Properties of Ti1+xS2 Prepared by CS2 Sulfurization. *Acta Mater.* **2012**, *60*, 7232−7240.

(6) Daou, R.; Takahashi, H.; Hébert, S.; Beaumale, M.; Guilmeau, E.; Maignan, A. Intrinsic Effects of Substitution and Intercalation on Thermal Transport in Two-Dimensional TiS2 Single Crystals. *J. Appl. Phys.* **2015**, *117*, 165101.

(7) Guelou, G.; Vaqueiro, P.; Prado-Gonjal, J.; Barbier, T.; Hebert, S.; Guilmeau, E.; Kockelmann, W.; Powell, A. V. The Impact of Charge Transfer and Structural Disorder on the Thermoelectric Properties of Cobalt Intercalated TiS2. *J. Mater. Chem. C* **2016**, *4*, 1871−1880.

(8) Hébert, S.; Berthebaud, D.; Daou, R.; Bréard, Y.; Pelloquin, D.; Guilmeau, E.; Gascoin, F.; Lebedev, O.; Maignan, A. Searching For New Thermoelectric Materials: Some Examples Among Oxides, Sulfides and Selenides. *J. Phys.: Condens. Matter* **2016**, *28*, 013001.

(9) Guilmeau, E.; Barbier, T.; Maignan, A.; Chateigner, D. Thermoelectric Anisotropy and Texture of Intercalated TiS2. *Appl. Phys. Lett.* **2017**, *111*, 133903.

(10) Beaumale, M.; Barbier, T.; Bréard, Y.; Guelou, G.; Powell, A.; Vaqueiro, P.; Guilmeau, E. Electron Doping and Phonon Scattering in Ti1+xS2 Thermoelectric Compounds. *Acta Mater.* **2014**, *78*, 86−92.

(11) Wan, C.; Gu, X.; Dang, F.; Itoh, T.; Wang, Y.; Sasaki, H.; Kondo, M.; Koga, K.; Yabuki, K.; Snyder, G. J.; et al. Flexible n-Type Thermoelectric Materials by Organic Intercalation of Layered Transition Metal Dichalcogenide TiS2. *Nat. Mater.* **2015**, *14*, 622−627.

(12) Wan, C.; Tian, R.; Kondou, M.; Yang, R.; Zong, P.; Koumoto, K. Ultrahigh Thermoelectric Power Factor in Flexible Hybrid Inorganic-Organic Superlattice. *Nat. Commun.* **2017**, *8*, 1024.

(13) Wan, C.; Wang, Y.; Wang, N.; Norimatsu, W.; Kusunoki, M.; Koumoto, K. Intercalation: Building a Natural Superlattice for Better Thermoelectric Performance in Layered Chalcogenides. *J. Electron. Mater.* **2011**, *40*, 1271−1280.

(14) Meakin, J. I.; Klipstein, P. C.; Friend, R. H. Transport and Magnetic Properties of Ag1/3TiS2. *J. Phys. C: Solid State Phys.* **1987**, *20*, 271.

(15) Chen, C. H.; Fabian, W.; Brown, F. C.; Woo, K. C.; Davies, B.; DeLong, B.; Thompson, A. H. Angle-Resolved Photoemission Studies of the Band Structure of $TiSe_2$ and TiS_2. *Phys. Rev. B: Condens. Matter Mater. Phys.* **1980**, *21*, 615−624.

(16) Greenaway, D.; Nitsche, R. Preparation and Optical Properties of Group IV−VI_2 Chalcogenides Having the CdI_2 Structure. *J. Phys. Chem. Solids* **1965**, *26*, 1445−1458.

(17) Klipstein, P. C.; Friend, R. H. Semiconductor to Semimetal Transition TiS_2 at 40 kbar. *J. Phys. C: Solid State Phys.* **1984**, *17*, 2713.

(18) Friend, R. H.; Jerome, D.; Liang, W. Y.; Mikkelsen, C.; Yoffe, A. D. Semimetallic Character of TiSe2 and Semiconductor Character of TiS2 Under Pressure. *J. Phys. C: Solid State Phys.* **1977**, *10*, L705.

DOI: 10.1021/acs.jpcc.8b08099
J. Phys. Chem. C 2018, 122, 26835−26844

(19) Thompson, A. H.; Pisharody, K. R.; Koehler, R. F. Experimental Study of the Solid Solutions $Ti_xTa_{1-x}S_2$. *Phys. Rev. Lett.* **1972**, *29*, 163−166.
(20) Lucovsky, G.; White, R. M.; Benda, J. A.; Revelli, J. F. Infrared-Reflectance Spectra of Layered Group-IV and Group-VI Transition-Metal Dichalcogenides. *Phys. Rev. B* **1973**, *7*, 3859−3870.
(21) Fischer, D. W. X-Ray Band Spectra and Electronic Structure of TiS_2. *Phys. Rev. B* **1973**, *8*, 3576−3582.
(22) Klipstein, P. C.; Bagnall, A. G.; Liang, W. Y.; Marseglia, E. A.; Friend, R. H. Stoichiometry Dependence of the Transport Properties of TiS2. *J. Phys. C: Solid State Phys.* **1981**, *14*, 4067.
(23) Traving, M.; Seydel, T.; Kipp, L.; Skibowski, M.; Starrost, F.; Krasovskii, E. E.; Perlov, A.; Schattke, W. Combined Photoemission and Inverse Photoemission Study of HfS_2. *Phys. Rev. B: Condens. Matter Mater. Phys.* **2001**, *63*, 035107.
(24) Lee, P.; Said, G.; Davis, R.; Lim, T. On the Optical Properties of Some Layer Compounds. *J. Phys. Chem. Solids* **1969**, *30*, 2719−2729.
(25) Allan, D. R.; Kelsey, A. A.; Clark, S. J.; Angel, R. J.; Ackland, G. J. High-Pressure Semiconductor-Semimetal Transition in TiS_2. *Phys. Rev. B: Condens. Matter Mater. Phys.* **1998**, *57*, 5106−5110.
(26) Fang, C. M.; de Groot, R. A.; Haas, C. Bulk and Surface Electronic Structure of 1T-TiS_2 and 1T-$TiSe_2$. *Phys. Rev. B: Condens. Matter Mater. Phys.* **1997**, *56*, 4455−4463.
(27) Reshak, A. H.; Auluck, S. Electronic and Optical Properties of the 1*T* Phases of TiS_2,$TiSe_2$, and $TiTe_2$. *Phys. Rev. B: Condens. Matter Mater. Phys.* **2003**, *68*, 245113.
(28) Reshak, A.; Auluck, S. Theoretical Investigation of the Electronic and Optical Properties of ZrX2 (X = S, Se and Te). *Phys. B* **2004**, *353*, 230−237.
(29) Sánchez, K.; Palacios, P.; Wahnón, P. Electronic Structure of Bulk- and Na-intercalated TiS_2Determined from a GGA+U Study with the Hubbard Terms Obtained Ab Initio. *Phys. Rev. B: Condens. Matter Mater. Phys.* **2008**, *78*, 235121.
(30) Dolui, K.; Sanvito, S. Dimensionality-Driven Phonon Softening and Incipient Charge Density Wave Instability in TiS2. *Europhys. Lett.* **2016**, *115*, 47001.
(31) Jiang, H. Structural and Electronic Properties of ZrX2 and HfX2 (X = S and Se) from First Principles Calculations. *J. Chem. Phys.* **2011**, *134*, 204705.
(32) Yumnam, G.; Pandey, T.; Singh, A. K. High Temperature Thermoelectric Properties of Zr and Hf Based Transition Metal Dichalcogenides: a First Principles Study. *J. Chem. Phys.* **2015**, *143*, 234704.
(33) Pike, N. A.; Dewandre, A.; Van Troeye, B.; Gonze, X.; Verstraete, M. J. Vibrational and Dielectric Properties of the Bulk Transition Metal Dichalcogenides. *Phys. Rev. Mater.* **2018**, *2*, 063608.
(34) Dovesi, R.; Orlando, R.; Erba, A.; Zicovich-Wilson, C. M.; Civalleri, B.; Casassa, S.; Maschio, L.; Ferrabone, M.; De La Pierre, M.; D'Arco, P.; et al. CRYSTAL14:A Program for the Ab Initio Investigation of Crystalline Solids. *Int. J. Quantum Chem.* **2014**, *114*, 1287−1317.
(35) Adamo, C.; Barone, V. Toward Reliable Density Functional Methods without Adjustable Parameters: The PBE0Model. *J. Chem. Phys.* **1999**, *110*, 6158.
(36) Weigend, F.; Ahlrichs, R. Balanced Basis Sets of Split Valence, Triple Zeta Valence and Quadruple Zeta Valence Quality for H to Rn: Design and Assessment of Accuracy. *Phys. Chem. Chem. Phys.* **2005**, *7*, 3297−305.
(37) Grimme, S.; Antony, J.; Ehrlich, S.; Krieg, H. A Consistent and Accurate Ab Initio Parametrization of Density Functional Dispersion Correction (DFT-D) for the 94 Elements H-Pu. *J. Chem. Phys.* **2010**, *132*, 154104.
(38) Grimme, S.; Ehrlich, S.; Goerigk, L. Effect of the Damping Function in Dispersion Corrected Density Functional Theory. *J. Comput. Chem.* **2011**, *32*, 1456−1465.
(39) Monkhorst, H. J.; Pack, J. D. Special Points for Brillouin-Zone integrations. *Phys. Rev. B* **1976**, *13*, 5188−5192.
(40) Setyawan, W.; Curtarolo, S. High-Throughput Electronic Band Structure Calculations: Challenges and Tools. *Comput. Mater. Sci.* **2010**, *49*, 299−312.
(41) Pascale, F.; Zicovich-Wilson, C. M.; Gejo, F. L.; Civalleri, B.; Orlando, R.; Dovesi, R. The Calculation of the Vibrational Frequencies of Crystalline Compounds and its Implementation in the CRYSTAL Code. *J. Comput. Chem.* **2004**, *25*, 888−897.
(42) Zicovich-Wilson, C. M.; Pascale, F.; Roetti, C.; Saunders, V. R.; Orlando, R.; Dovesi, R. Calculation of the Vibration Frequencies Of Alpha-Quartz: the Effect of Hamiltonian and Basis Set. *J. Comput. Chem.* **2004**, *25*, 1873−1881.
(43) Maschio, L.; Kirtman, B.; Rérat, M.; Orlando, R.; Dovesi, R. Ab Initio Analytical Raman Intensities for Periodic Systems through a Coupled Perturbed Hartree-Fock/Kohn-Sham Method in an Atomic Orbital Basis. I. Theory. *J. Chem. Phys.* **2013**, *139*, 164101.
(44) Maschio, L.; Kirtman, B.; Rérat, M.; Orlando, R.; Dovesi, R. Ab Initio Analytical Raman Intensities for Periodic Systems through a Coupled Perturbed Hartree-Fock/Kohn-Sham Method in an Atomic Orbital Basis. II. Validation and Comparison with Experiments. *J. Chem. Phys.* **2013**, *139*, 164102.
(45) Togo, A.; Oba, F.; Tanaka, I. First-Principles Calculations of the Ferroelastic Transition between Rutile-Type and $CaCl_2$-Type SiO_2at High Pressures. *Phys. Rev. B: Condens. Matter Mater. Phys.* **2008**, *78*, 134106.
(46) Togo, A.; Tanaka, I. First Principles Phonon Calculations in Materials Science. *Scr. Mater.* **2015**, *108*, 1−5.
(47) Lindroth, D. O.; Erhart, P. Thermal Transport in Van Der Waals Solids from First-Principles Calculations. *Phys. Rev. B: Condens. Matter Mater. Phys.* **2016**, *94*, 115205.
(48) Wang, Y.; Wang, J. J.; Wang, W. Y.; Mei, Z. G.; Shang, S. L.; Chen, L. Q.; Liu, Z. K. A Mixed-Space Approach to First-Principles Calculations of Phonon Frequencies for Polar Materials. *J. Phys.: Condens. Matter* **2010**, *22*, 202201.
(49) Madsen, G. K.; Singh, D. J. Boltztrap. A Code for Calculating Band-Structure Dependent Quantities. *Comput. Phys. Commun.* **2006**, *175*, 67−71.
(50) Beal, A. R.; Liang, W. Y. Intercalation Studies of Some Transition Metal Dichalcogenides. *Philos. Mag.* **1973**, *27*, 1397−1416.
(51) Inoue, M.; Negishi, H. Chemical Vapor Growth and Manganese Metal Intercalation of TiS2. *J. Phys. Soc. Jpn.* **1984**, *53*, 943−946.
(52) Kusawake, T.; Takahashi, Y.; Ohshima, K.-I. Structural Analysis of the Layered Compounds Cu_xTiS2. *Mol. Cryst. Liq. Cryst. Sci. Technol., Sect. A* **2000**, *341*, 93−98.
(53) McTaggart, F.; Wadsley, A. The sulphides, Selenides, and Tellurides of Titanium, Zirconium, Hafnium, and Thorium. I. Preparation and Characterization. *Aust. J. Chem.* **1958**, *11*, 445−457.
(54) Björkman, T.; Gulans, A.; Krasheninnikov, A. V.; Nieminen, R. M. van der Waals Bonding in Layered Compounds from Advanced Density-Functional First-Principles Calculations. *Phys. Rev. Lett.* **2012**, *108*, 235502.
(55) Imai, H.; Shimakawa, Y.; Kubo, Y. Large Thermoelectric Power Factor in TiS_2Crystal with Nearly Stoichiometric Composition. *Phys. Rev. B: Condens. Matter Mater. Phys.* **2001**, *64*, 241104.
(56) Madsen, G. K. H. Automated Search for New Thermoelectric Materials: The Case of LiZnSb. *J. Am. Chem. Soc.* **2006**, *128*, 12140−12146.
(57) Tadano, T.; Tsuneyuki, S. First-Principles Lattice Dynamics Method for Strongly Anharmonic Crystals. *J. Phys. Soc. Jpn.* **2018**, *87*, 041015.
(58) Barry, J. J.; Hughes, H. P.; Klipstein, P. C.; Friend, R. H. Stoichiometry Effects in Angle - Resolved Photoemission and Transport Studies of $Ti_{1+X}S_2$. *J. Phys. C: Solid State Phys.* **1983**, *16*, 393.
(59) Sandoval, S. J.; Chen, X. K.; Irwin, J. C. Raman Spectra of $Ag_x$$TiS_2$and Lattice Dynamics of.$TiS_2$. *Phys. Rev. B: Condens. Matter Mater. Phys.* **1992**, *45*, 14347−14353.

DOI: 10.1021/acs.jpcc.8b08099
J. Phys. Chem. C 2018, 122, 26835−26844

(60) Ding, H.; Xu, B. Structural, Elastic, and Vibrational Properties of Layered Titanium Dichalcogenides: A Van Der Waals Density Functional Study. *J. Chem. Phys.* **2012**, *137*, 224509.
(61) Roubi, L.; Carlone, C. Resonance Raman Spectrum of $HfS_2$and.ZrS_2. *Phys. Rev. B: Condens. Matter Mater. Phys.* **1988**, *37*, 6808−6812.
(62) Mañas-Valero, S.; García Lopez, V.; Cantarero, A.; Galbiati, M. Raman Spectra of ZrS2 and ZrSe2 from Bulk to Atomically Thin Layers. *Appl. Sci.* **2016**, *6*, 264.
(63) Cingolani, A.; Lugarà, M.; Lévy, F. Resonance Raman Scattering in HfSe2 and HfS2. *Phys. Scr.* **1988**, *37*, 389.
(64) Iwasaki, T.; Kuroda, N.; Nishina, Y. Anisotropy of Lattice Dynamical Properties in ZrS2 and HfS2. *J. Phys. Soc. Jpn.* **1982**, *51*, 2233−2240.
(65) Chen, J. Phonons in Bulk and Monolayer HfS2 and Possibility of Phonon-Mediated Superconductivity: A First-Principles Study. *Solid State Commun.* **2016**, *237*−*238*, 14−18.
(66) Lucovsky, G.; Liang, W.; White, R.; Pisharody, K. Reflectivity Studies of Ti- and Ta-Dichalcogenides: Phonons. *Solid State Commun.* **1976**, *19*, 303−307.
(67) Vaterlaus, H. P.; Levy, F. Phonons and Free Carriers in Group IVB Transition-Metal Dichalcogenides. *J. Phys. C: Solid State Phys.* **1985**, *18*, 2351.
(68) Manzeli, S.; Ovchinnikov, D.; Pasquier, D.; Yazyev, O. V.; Kis, A. 2D Transition Metal Dichalcogenides. *Nat. Rev. Mater.* **2017**, *2*, 17033.
(69) Sugai, S. Lattice Vibrations in the Charge-Density-Wave States of Layered Transition Metal Dichalcogenides. *Phys. Status Solidi B* **1985**, *129*, 13−39.
(70) Wilson, J. A.; di Salvo, F. J.; Mahajan, S. Charge-Density Waves and Superlattices in the Metallic Layered Transitiosn Metal Dichalcogenides. *Adv. Phys.* **1975**, *24*, 117−201.
(71) Hossain, M.; Zhao, Z.; Wen, W.; Wang, X.; Wu, J.; Xie, L. Recent Advances in Two-Dimensional Materials with Charge Density Waves: Synthesis, Characterization and Applications. *Crystals* **2017**, *7*, 298.
(72) Van Bakel, G. P. E. M.; De Hosson, J. T. M. Various Regimes of Charge-Density Waves in Layered Compounds. *Phys. Rev. B: Condens. Matter Mater. Phys.* **1992**, *46*, 2001.

DOI: 10.1021/acs.jpcc.8b08099
J. Phys. Chem. C 2018, 122, 26835−26844